Electronic and Molecular Structures of Pentaammineruthenium Pyridine and Benzonitrile Complexes as a Function of Oxidation State

Yeung-gyo K. Shin, David J. Szalda,† Bruce S. Brunschwig,* Carol Creutz,* and Norman Sutin*

Chemistry Department, Brookhaven National Laboratory, P.O. Box 5000, Upton, New York 11973-5000

Received January 29, 1997[⊗]

The structural characterization of both Ru(II) and Ru(III) compounds containing $Ru(NH_3)_5^{2+/3+}$ with pyridine or benzonitrile as the sixth ligand (L) is described. Crystal data for L = pyridine, $[(NH_3)_5Ru(NC_5H_5)](SO_3CF_3)_2$ (**1**): orthorhombic space group *Pbcn*, $Z = 4$, $a = 13.096(2)$ Å, $b = 11.541(2)$ Å, $c = 13.179(2)$ Å. For $[(NH_3)_5Ru(NC_5H_5)]Cl_3 \cdot 1.4H_2O$ (**2**): orthorhombic space group *Pnma*, $Z = 4$, $a = 22.667(12)$ Å, $b = 7.095(2)$ Å, $c = 10.097(8)$ Å. For L = benzonitrile, $[(NH_3)_5Ru(NCC_6H_5)](SO_3CF_3)_2$ (**3**): monoclinic space group $P2_1/n$, $Z = 4$, $a = 9.561(1)$ Å, $b = 18.424(4)$ Å, $c = 12.181(1)$ Å, $\beta = 95.73(1)°$. For $[(NH_3)_5Ru(NCC_6H_5)](S_2O_6)_{3/2} \cdot 2H_2O$ (**4**): triclinic space group $P\bar{1}$, $Z = 2$, $a = 7.8947(6)$ Å, $b = 11.517(2)$ Å, $c = 11.630(1)$ Å, $\alpha = 99.61(1)°$, $\beta = 97.275(8)°$, $\gamma = 102.25(1)°$. The $Ru^{II}-N(L)$ and $Ru^{III}-N(L)$ distances are respectively 2.058(8) and 2.077(10) Å for L = pyridine and 1.945(5) and 2.025(4) Å for L = benzonitrile. The new data yield a comprehensive set of structural parameters for modeling and interpreting electron transfer barriers and for investigating the dependence of metal−ligand coupling on d_{M-N}, for which the results of INDO calculations are also reported here.

Mononuclear ruthenium pentaammine L complexes have served as valuable tools in many outer-sphere electron transfer studies, and binuclear, mixed-valence ligand-bridged pentaammineruthenium complexes have contributed much to the understanding of electron transfer barriers and electronic coupling elements through their rich spectroscopy. The two most common "lead-in" functions in both series are pyridyl and nitrile groups. Despite the centrality of these structural features, few structural data have been available. Structural data are important in understanding electron transfer barriers and donor/acceptor electronic coupling. Bond distance and angle differences between the oxidized and reduced forms of a complex determine the inner-shell reorganizational barrier, while metal−ligand distances reflect/influence the degree of metal−ligand coupling and, hence, metal−metal coupling in the case of the mixed-valence complexes. In previous work, structural data as a function of metal oxidation state have been reported for $Ru(NH_3)_5L$ (L = NH_3,[1] pz,[2] and $pz(CH_3^+)$[3]) and $Ru(NH_3)_4L_2$ (L = py-4-$(CONH_2)$[4]). In the present study, the $Ru(NH_3)_5L$ pairs with L = py and NCC_6H_5 are reported. The new data yield a comprehensive set of structural parameters for modeling and interpreting electron transfer barriers and for investigating the dependence of metal−ligand coupling on d_{M-N}, for which the results of INDO calculations are also reported here.

Experimental Section

The $Ru(NH_3)_5L$ complexes (L = py[5] and NCC_6H_5[6]) were prepared and characterized by published methods.

Pyridine Complexes. Crystals of the Ru(II) complex $[(NH_3)_5Ru(py)](SO_3CF_3)_2$ (**1**) were prepared by dissolving 50 mg of **1** in 2 mL of water and layering this solution on top of a saturated solution of $LiSO_3CF_3$ in a vial. The vial was placed in a desiccator containing Drierite and stored in a refrigerator. After several days, orange prisms suitable for X-ray analysis were formed. Crystals of the Ru(III) complex $[(NH_3)_5Ru(py)]Cl_3 \cdot 1.4H_2O$ (**2**) were prepared by dissolving 30 mg of **2** in 1 mL of water containing 2 drops of 1 M HCl. This solution was layered on top of 2 mL of 2.5 M NaCl. The vial was placed in a desiccator containing Drierite and stored in a refrigerator. After several days, a few light yellow prisms suitable for X-ray analysis were formed.

Benzonitrile Complexes. Crystals of the Ru(II) complex $[(NH_3)_5Ru(NCC_6H_5)](SO_3CF_3)_2$ (**3**) were prepared by dissolving 10 mg of **3** in 2 mL of 1 M $LiSO_3CF_3$. The vial was placed in a desiccator containing Drierite and stored in a refrigerator. After several days, yellow crystals suitable for X-ray analysis were formed. Crystals of the Ru(III) complex $[(NH_3)_5Ru(NCC_6H_5)](S_2O_6)_{3/2} \cdot 2H_2O$ (**4**) were prepared by dissolving 33.4 mg of **3** in 2 mL of water and adding 7.68 mg of $K_2S_2O_8$, followed by 0.5 mL of 0.1 M sulfuric acid. The vial was placed in a desiccator containing Drierite and stored in a refrigerator. Yellow crystals suitable for X-ray analysis were formed after several days.

Collection and Reduction of X-ray Data. Crystals of **1** were orange prisms. A crystal 0.40 mm × 0.30 mm × 0.25 mm was coated with petroleum jelly and mounted in a glass capillary tube. The diffraction data indicated the crystal to be orthorhombic with systematic absences $0kl$, $l = 2n + 1$, $h0l$, $h = 2n + 1$, and $hk0$, $h + k = 2n + 1$, consistent with space group *Pcan*, a nonstandard setting of *Pbcn*.[7] The data were collected using space group *Pcan* but were then reindexed to conform to space group *Pbcn;* the structure was solved, refined, and reported using *Pbcn*.

Crystals of **2** were light yellow prisms. A crystal 0.14 mm × 0.18 mm × 0.40 mm was coated with petroleum jelly and placed in a capillary tube. The diffraction data indicated orthorhombic symmetry with sytematic absences $0kl$, $l = 2n + 1$, and $hk0$, $h + k = 2n + 1$, consistent with space groups $Pc2_1n$ and *Pcmn*. The data were collected and the structure solved using these space groups, and the data were then reindexed to be consistent with the standard centrosymetric space group *Pnma*.[8]

Crystals of **3** suitable for X-ray analysis were yellow prisms. A crystal 0.28 mm × 0.30 mm × 0.40 mm was used for data collection.

† To whom questions regarding the X-ray crystallography should be directed. Permanent address: Department of Natural Science, Baruch College, Manhattan, NY 10010.

⊗ Abstract published in *Advance ACS Abstracts,* June 15, 1997.

(1) Stynes, H. C.; Ibers, J. A. *Inorg. Chem.* **1971**, *10*, 2304−2308.
(2) Gress, M. E.; Creutz, C.; Quicksall, C. O. *Inorg. Chem.* **1981**, *20*, 1522−1528.
(3) Wishart, J. F.; Bino, A.; Taube, H. *Inorg. Chem.* **1986**, *25*, 3318−3321.
(4) Richardson, D. E.; Walker, D. E.; Sutton, J. E.; Hodgson, K. O.; Taube, H. *Inorg. Chem.* **1979**, *18*, 2216−2221.
(5) Gaunder, R. G.; Taube, H. *Inorg. Chem.* **1970**, *9*, 2627−2639.
(6) Zanella, A. W.; Ford, P. C. *Inorg. Chem.* **1975**, *14*, 42−47.
(7) *International Tables for X-ray Crystallography*, 3rd ed.; Kynoch Press: Birmingham, UK, 1969; Vol. I, p 149.

S0020-1669(97)00096-7 CCC: $14.00

Table 1. Crystallographic Data, Experimental Conditions, and Refinements for Complexes **1**−**4**

	1	**2**	**3**	**4**
formula	$C_7S_2F_6H_{20}N_6O_6Ru$	$C_5Cl_3H_{22.8}N_6O_{1.4}Ru$	$C_9S_2F_6H_{20}N_6O_6Ru$	$C_7S_3H_{24}N_6O_{11}Ru$
fw	563.45	396.90	563.45	541.36
space group	*Pbcn* (No. 60)	*Pnma* (No. 62)	$P2_1/n$ (No. 14)	$P\bar{1}$ (No. 2)
a (Å)	13.096(2)	22.667(12)	9.561(1)	7.8947(6)
b (Å)	11.541(2)	7.095(2)	18.424(4)	11.517(2)
c (Å)	13.179(2)	10.097(8)	12.181(1)	11.630(1)
α (deg)				99.61(1)
β (deg)			95.73(1)	97.275(8)
γ (deg)				102.25(1)
V (Å^3)	1991.9(6)	1623 (2)	2135.0(6)	1004.3(2)
Z	4	4	4	2
ρ_{calcd} (g cm^{-3})	1.879	1.624	1.753	1.790
radiation; *λ* (Å)	0.71069 (Mo Kα)	0.71069 (Mo Kα)	0.71069 (Mo Kα)	0.71069 (Mo Kα)
μ (cm^{-1})	10.6	14.4	9.89	11.9
transm coeff	0.7360−0.7904	0.6596−0.8318	0.6831−0.8047	0.7870−0.9604
R^a	0.053	0.071	0.051	0.043
$R_w{}^b$	0.069	0.075	0.061	0.040
Δ/*σ* (max)	≤0.2	≤0.01	≤0.02	≤0.02
T (K)	295	294	295	295

^{a} $R = \sum||F_o| - |F_c||/\sum|F_o|$. ^{b} $R_w = \{\sum[w(|F_o| - |F_c|)^2]/\sum[w|F_o|^2]\}^{1/2}$.

The crystal was coated with petroleum jelly and mounted in a glass capillary tube. A monoclinic unit cell was obtained with systematic absences $0k0$, $k = 2n + 1$, and $h0l$, $h + l = 2n + 1$, consistent with space group $P2_1/n$, a nonstandard setting of $P2_1/c$.[9]

Crystals of **4** were pale yellow prisms, and a crystal 0.04 mm × 0.23 mm × 0.57 mm was coated with petroleum jelly and sealed in a glass capillary. The diffraction data indicated triclinic symmetry, and space group $P\bar{1}$[10] was assumed for the solution and refinement of the structure.

Crystal data and information on data collection using an Enraf Nonius CAD4 diffractometer for all four structures are given in Table 1 and, in detail, in Table S1 of the Supporting Information.

Determination and Refinement of Structure. The structures were solved by standard Patterson heavy-atom methods.[11] In the full-matrix least-squares refinement, neutral-atom scattering factors[12] and corrections for anomalous dispersion[13] were used, and the quantity $\sum w(|F_o| - |F_c|)^2$ was minimized. For all four structures, anisotropic temperature parameters were used for all the non-hydrogen atoms (except for atoms with occupancy factors less than 0.5). For **1** and **2** during the final cycles of refinement, the hydrogen atoms on the pyridine ligand were introduced in their calculated positions (C−H = 0.95 Å) and allowed to "ride" [11] on the C atom to which they were bound. In **1**, the hydrogen atoms on the coordinated ammines were located on a difference Fourier map and included at these fixed positions. The hydrogen atoms on the ammines in **2** were not included in the refinement. A common isotropic thermal parameter was refined for all of the pyridine hydrogen atoms in **1** and **2**. In **1**, a second common thermal parameter was used for the ammine hydrogen atoms. The hydrogen atoms in **3** and **4** were found on difference Fourier maps, and their positional (except for H(5) in **3**, which was included at a calculated position) and isotropic thermal parameters were refined (a common isotropic thermal parameter in **3** and individual isotropic thermal parameters in **4**). The atomic coordinates for the non-hydrogen atoms are listed in Tables S2−S5 (Supporting Information).

Energy Calculations. Reorganization and electronic energy calculations were carried out using ZINDO-95. Both the spectroscopic and the ground-state geometry optimization INDO models of Zerner and co-workers were employed.[14] For the spectroscopic INDO calculations, the Mataga−Nishimoto *γ* values and the interaction factors 1.0, 1.267, 0.585, 1.0, 1.0, and 1.0 were used for s_σ, p_σ, p_π, d_σ, d_π, and d_δ, respectively. Theoretical *γ* values and interaction factors of 1.0 were employed for the ground-state surfaces and the geometry optimizations. Default resonance integral parameters were used, except in the following cases: oxygen, $\beta(2s) = \beta(2p) = -54.0$ eV, and ruthenium, $\beta(5s) = \beta(5p) = -1.00$ eV, $\beta(4d) = -26.29$ eV. Reorganization energies were also calculated using the molecular mechanics[15a] application of the CAChe programs.[15b] CAChe molecular mechanics augments the MM2 force field designated developed by Allinger[16] by providing rules for estimating parameters for cases not addressed by MM2. The augmented force field uses a stretching force constant of 4.4×10^5 dyn cm^{-1} for the Ru−N bonds and d_o values of 2.28 and 2.006 Å for the Ru−NH_3 and Ru−N(L) bond lengths, respectively.

Results and Discussion

Structures. A view of $(NH_3)_5Ru(py)^{2+}$ in **1**, along with the numbering scheme used for **1** and **2**, is presented in Figure 1. The ruthenium is coordinated to five ammonias, with the pyridine ligand completing the octahedral coordination sphere. The ruthenium, N(2), N(1), and C(4) lie on a crystallographic twofold axis. The $(NH_3)_5Ru(py)^{3+}$ in **2** is essentially the same as in **1**, except that the crystallographic mirror plane contains the ruthenium, N(2), and all the atoms in the pyridine ligand. Table 2 lists the metal−ligand bond distances and angles for **1** and **2**. In $(NH_3)_5Ru(py)^{2+}$, the Ru−N(py) bond distance is 2.058(8) Å, and the average Ru−NH_3 bond distance is 2.145(8) Å. A small trans effect is also observed. In $(NH_3)_5Ru$-

(8) *International Tables for X-ray Crystallography*, 3rd ed.; Kynoch Press: Birmingham, UK, 1969; Vol. I, p 151.
(9) *International Tables for X-ray Crystallography*, 3rd ed.; Kynoch Press: Birmingham, UK, 1969; Vol. I, p 99.
(10) *International Tables for X-ray Crystallography*, 3rd ed.; Kynoch Press: Birmingham, UK, 1969; Vol. I, p 75.
(11) Sheldrick, G. M. SHELX 76: Crystal Structure Refinement Program. Cambridge University, Cambridge, England, 1976.
(12) *International Tables for X-ray Crystallography*, 3rd ed.; Kynoch Press: Birmingham, UK, 1974; Vol. IV, pp 99−100.
(13) Cromer, D. T.; Liberman, D. *J. Chem. Phys.* **1970**, *53*, 1891−1898.
(14) (a) ZINDO is an implementation of intermediate neglect of differential overlap (INDO) semiempirical quantum mechanical methods[14f] to solve the Schrodinger equation for a molecule. The implementation does not yield an exact solution for the molecule but rather approximates certain of the integrals semiempirically. (b) Zerner, M. C. The ZINDO Quantum Chemistry Package. University of Florida, Gainesville, FL, 1995. (c) Zerner, M. C.; Loew, G. H.; Kirchner, R. F.; Müller-Westerhoff, U. T. *J. Am. Chem. Soc.* **1980**, *102*, 589−599. (d) Ridley, J. E.; Zerner, M. C. *Theor. Chim. Acta* **1973**, *32*, 111−134. (e) Bacon, A. D.; Zerner, M. C. *Theor. Chim. Acta* **1979**, *53*, 21−54. (f) Pople, J. A.; Beveridge, D. L. *Approximate Molecular Orbital Theory*; McGraw Hill: New York, 1970.
(15) (a) Molecular mechanics refers to a method of determining the relative energy of a particular nuclear configuration of a molecule by using the classical Newtonian equations of motion. The method models the molecule as a set of atoms constrained by "springs". Thus, a force field is developed that has force constants for stretches, bends, etc. for the relative motion of the atoms. Different force fields have been implemented and parametrized by a number of authors. (b) CAChe Scientific, Version 3.6, Oxford Molecular Group, Inc., Campbell, CA, 1993.
(16) Allinger, N. L. *J. Am. Chem. Soc.* **1977**, *99*, 8127−8134.

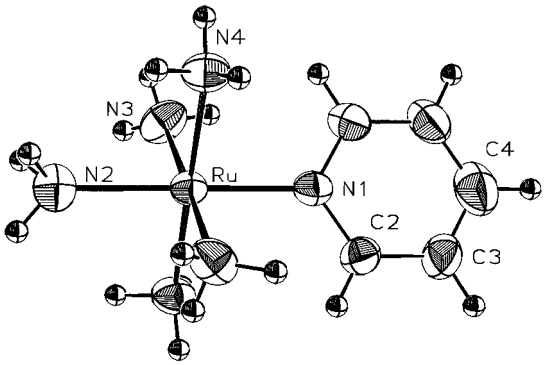

Figure 1. ORTEP drawing of $(NH_3)_5Ru^{II}(py)^{2+}$ in **1.** The thermal ellipsoids are at the 50% probability level, and the hydrogen atoms are included. The atom labeling scheme is used for both **1** and **2**. The ruthenium atom, N(2), N(1), and C(4) lie on a crystallographic twofold axis which relates the labeled atoms to the unlabeled atoms.

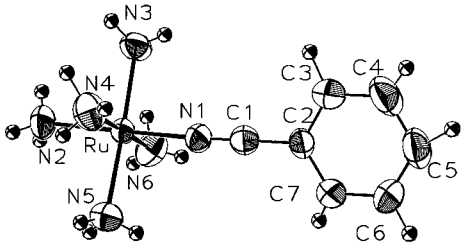

Figure 2. ORTEP drawing of $(NH_3)_5Ru^{II}(NCC_6H_5)^{2+}$ in **3**. The thermal ellipsoids are at the 50% probability level and the hydrogen atoms are included. The atom labeling scheme is used for both **3** and **4**.

$(py)^{3+}$, the Ru−N(py) bond distance is 2.077(10) Å, and the average Ru−NH_3 bond distance is 2.109(9) Å. In both complexes, the plane of the pyridine lies between the two ammines, with the dihedral angles between the plane of the pyridine and the plane formed by Ru, N(1), N(2), and N(3) and Ru, N(1), N(2), and N(4) being 42.6° and 48.9°, respectively, in **1**, while they are equal in **2**.

Figure 2 depicts $(NH_3)_5Ru(NCC_6H_5)^{2+}$ in **3**, along with the numbering scheme used for **3** and **4**. The structures of $(NH_3)_5Ru(NCC_6H_5)^{2+}$ and $(NH_3)_5Ru(NCC_6H_5)^{3+}$ (in **4**) are similar to those of $(NH_3)_5Ru(py)^{2+}$ and $(NH_3)_5Ru(py)^{3+}$. The Ru^{II}−$N(NCC_6H_5)$ bond length is 1.954(5) Å, and the average Ru^{II}−NH_3 bond length is 2.126(8) Å in **3**. The Ru^{III}−$N(NCC_6H_5)$ bond length is 2.025(4) Å, and the average Ru^{III}−NH_3 bond length is 2.091(6) Å in **4**. In **3**, the dihedral angles between the plane of the phenyl ring and the plane formed by Ru, N(1), N(2), and N(5) and Ru, N(1), N(2), and N(6) are 24.3° and 65.9°, respectively, while they are 79.2° and 11.5°, respectively, in **4**.

Ruthenium−nitrogen bond lengths for Ru(II) and Ru(III) ammine complexes are compared in Table 3. The Ru−N(L) bond distances are *shorter* for the Ru(II) complexes and show relatively larger variations with L (from 2.06 Å for L = py to 1.95 Å for L = NCC_6H_5 and $pz(CH_3^+)$), consistent with the importance of ligand-dependent π back-bonding between the $(NH_3)_5Ru^{2+}$ center and L and less steric hindrance toward close approach of NCC_6H_5. By contrast, the Ru^{III}−N(L) bond distances are about 2.08 Å for L = py, pz, and $pz(CH_3^+)$, the shorter bond distance of 2.025 Å for the benzonitrile complex presumably again reflecting less steric hindrance. The role which the other ligands play in controlling the extent of the Ru^{II}−N(L) back-bonding can be seen by comparing $(NH_3)_5Ru(py)^{2+}$ with $[Ru(2,2'\text{-bpy})(terpy)(4,4'\text{-bpy})Ru(NH_3)_5]^{4+}$ [17]

(17) Szalda, D. J.; Fagalde, F.; Katz, N. E. *Acta Crystallogr.* **1996**, *C52*, 3013−3016.

Table 2. Comparison of Selected Bond Distances (Å) and Angles (deg) for the Pyridine and Benzonitrile Complexes[a]

	$(NH_3)_5Ru(py)^{2+}$ (**1**)	$(NH_3)_5Ru(py)^{3+}$ (**2**)
	Ruthenium−Ligand Distances	
Ru−N(1)	2.058(8)	2.077(10)
Ru−N(2)	2.158(8)	2.100(9)
Ru−N(3)	2.139(6)	
Ru−N(4)	2.139(6)	2.123(6)
Ru−N(6)		2.105(6)
	Ruthenium−Ligand Angles	
N(1)−Ru−N(2)		179.8(1)
N(1)−Ru−N(3)	90.8(2)	
N(1)−Ru−N(4)	89.8(2)	91.1(3)
N(1)−Ru−N(6)		90.8(3)
N(2)−Ru−N(3)	89.2(2)	
N(2)−Ru−N(4)	90.2(2)	88.8(3)
N(2)−Ru−N(6)		89.3(3)
N(3)−Ru−N(4)	91.5(2)	92.0(3)
N(3)−Ru−N(6)		88.8(3)
N(4)−Ru−N(5)	178.4(2)	
N(4)−Ru−N(6)		177.9(3)
N(5)−Ru−N(6)		90.4(3)
	$(NH_3)_5Ru(NCC_6H_5)^{2+}$ (**3**)	$(NH_3)_5Ru(NCC_6H_5)^{3+}$ (**4**)
	Ruthenium−Ligand Distances	
Ru−N(1)	1.954(5)	2.025(4)
Ru−N(2)	2.122(6)	2.080(6)
Ru−N(3)	2.122(6)	2.092(5)
Ru−N(4)	2.124(8)	2.106(4)
Ru−N(5)	2.126(7)	2.091(5)
Ru−N(6)	2.135(8)	2.084(5)
	Ruthenium−Ligand Angles	
N(1)−Ru−N(2)	179.1(3)	178.6(3)
N(1)−Ru−N(3)	90.7(2)	87.7(2)
N(1)−Ru−N(4)	90.5(3)	89.6(2)
N(1)−Ru−N(5)	91.2(3)	91.6(2)
N(1)−Ru−N(6)	90.9(3)	89.8(2)
N(2)−Ru−N(3)	88.6(3)	90.9(3)
N(2)−Ru−N(4)	88.9(3)	90.2(2)
N(2)−Ru−N(5)	89.5(3)	89.8(3)
N(2)−Ru−N(6)	89.7(3)	90.4(2)
N(3)−Ru−N(4)	90.3(3)	89.1(2)
N(3)−Ru−N(5)	178.0(3)	178.7(2)
N(3)−Ru−N(6)	89.7(3)	90.5(2)
N(4)−Ru−N(5)	89.1(3)	89.8(2)
N(4)−Ru−N(6)	178.5(3)	179.3(3)
N(5)−Ru−N(6)	90.7(3)	90.6(2)

[a] For **1**, N(3) is related to N(5) and N(4) is related to N(6) by the twofold axis. For **2**, N(3) is related to N(4) and N(5) is related to N(6) by the mirror plane.

(bpy = bipyridine; terpy = 2,2′:6′,2″-terpyridine). In the latter complex, the $[(NH_3)_5Ru]$−N(4,4′-bpy) bond length is 2.052(7) Å, close to that observed in $(NH_3)_5Ru(py)^{2+}$, while the other Ru−N(4,4′-bpy) bond length is 2.112(7) Å. This difference is due to the greater π-basicity of $Ru(NH_3)_5^{2+}$. The bond length of 2.077(10) Å observed in $(NH_3)_5Ru(py)^{3+}$ is nearly identical to that of 2.076(8) in $(NH_3)_5Ru(pz)^{3+}$ [2] and is near the 2.115(1) Å observed in the binuclear complex $[(NH_3)_5Ru(pz)Ru(NH_3)_5]^{6+}$.[18]

Similarly, the Ru−$N(NCC_6H_5)$ bond length of 1.954(5) Å in $(NH_3)_5Ru(NCC_6H_5)^{2+}$ can be compared to the 2.119(11) Å observed in $(CO)_2(Cl)_2Ru(NCC_6H_5)_2$,[19] where the benzonitrile is trans to a carbonyl, and the 1.996(3) Å found in [bis(benzonitrile-*N*)(5,5,10,15,15,20-hexaethylporphyrin)ruthenium].[20] In [*trans*-bis(benzonitrile-*N*)tetrachlororuthenium]$^{1-}$ and

(18) Furholz, U.; Joss, S.; Burgi, H. B.; Ludi, A. *Inorg. Chem.* **1985**, *24*, 943−948.

(19) Daran, J. C.; Jeannin, Y.; Rigault, C. *Acta Crystallogr.* **1984**, *C40*, 249−251.

Table 3. Ru−N Distances (Å) from X-ray Crystallographic Measurements[a]

complex	d(Ru−N(L))	d(Ru−NH_3)	ref
$Ru(NH_3)_6^{2+}$		2.144(4) av	1
$Ru(NH_3)_6^{3+}$		2.104(4) av	1
$(NH_3)_5Ru^{II}(py)^{2+}$	2.058(8)	2.139(4) eq; 2.158(8) ax	*b*
$(NH_3)_5Ru^{III}(py)^{3+}$	2.077(10)	2.114(4) eq; 2.100(9) ax	*b*
$(NH_3)_5Ru^{II}(NCC_6H_5)^{2+}$	1.954(5)	2.128(4) eq; 2.122(6) ax	*b*
$(NH_3)_5Ru^{III}(NCC_6H_5)^{3+}$	2.025(4)	2.093(2) eq; 2.080(6) ax	*b*
$(NH_3)_5Ru^{II}(pz)^{2+}$	2.006(6)	2.153(3) eq; 2.166(7) ax	2
$(NH_3)_5Ru^{III}(pz)^{3+}$	2.076(8)	2.106(4) eq; 2.125(8) ax	2
$(NH_3)_5Ru^{II}(pzCH_3^+)^{3+}$	1.95(1)	2.129(6) eq; 2.17(1) ax	3
$(NH_3)_5Ru^{III}(pzCH_3^+)^{4+}$	2.08(1)	2.112(5) eq; 2.10(1) ax	3
cis-$(NH_3)_4Ru^{II}$(py-4-C(O)$NH_2)_2^{2+}$	2.058(6) av	2.155(11) av	4
cis-$(NH_3)_4Ru^{III}$(py-4-C(O)$NH_2)_2^{3+}$	2.099(4) av	2.125(7) av	4

[a] The values listed for the equatorial Ru−NH_3 distances are averages. [b] Determined in this study.

mer-tris(benzonitrile-*N*)trichlororuthenium,[21] the average Ru−N(NCC_6H_5) bond lengths are 2.013(3) and 2.026(9) Å, respectively, while it is 2.025(4) Å in $(NH_3)_5Ru(NCC_6H_5)^{3+}$.

The extent of the π back-bonding in $Ru(NH_3)_5^{2+}$ versus $Ru(NH_3)_5^{3+}$ complexes can also be observed in the difference between the Ru−N(py) and Ru−NH_3 bond lengths. For $(NH_3)_5Ru(py)^{2+}$, the difference is 0.087(8) Å, while for $(NH_3)_5Ru(py)^{3+}$, it is only 0.032(10) Å. This difference is 0.172(8) Å in $(NH_3)_5Ru(NCC_6H_5)^{2+}$ and 0.066(6) Å in $(NH_3)_5Ru(NCC_6H_5)^{3+}$.

Inner-Shell Reorganization Energies. The inner-shell reorganization barriers for the Ru(II)−Ru(III) self-exchanges can be calculated from the structures of the oxidized and reduced complexes and the appropriate force constants. Here we consider only the Ru−N bond distance changes and estimate the reorganization barriers from eq 1a, where f_i is the reduced

$$\Delta G^*_{in} = \lambda_{in}/4 = {}^1/_2\sum f_i[(\Delta d^0{}_i)/2]^2 \qquad (1a)$$

force constant for the ith Ru−N vibration ($f_i = 2f_{2i}\, f_{3i}/(f_{2i} + f_{3i})$, where f_2 and f_3 are the force constants for the Ru^{II}−N and Ru^{III}−N stretching vibrations, respectively) and $\Delta d^0{}_i$ is the difference between the equilibrium Ru^{II}−N and Ru^{III}−N bond lengths ($\Delta d^0 = d^0(Ru^{II}-N) - d^0(Ru^{III}-N)$).[22]

The frequency of the symmetrical Ru−N stretching vibration in $Ru(NH_3)_6^{3+}$ is[23] 500 cm^{-1}, corresponding to a Ru^{III}−NH_3 stretching force constant of 2.5×10^5 dyn cm^{-1}. Dividing this value by 1.28, the ratio of the (Ru^{III}−NH_3)/(Ru^{II}−NH_3) stretching force constants,[24] yields 1.95×10^5 dyn cm^{-1} for the Ru^{II}−NH_3 force constant and 2.2×10^5 dyn cm^{-1} for the reduced force constant for the Ru−NH_3 stretching vibration. The ratio of the (Ru^{II}−N(py))/(Ru^{II}−NH_3) force constants calculated from the Ru−N stretching frequencies using a rigid-ligand MX_6 model (and neglecting interactions with the trans Ru−N bonds) is 1.54.[25] Assuming similar Ru−N stretching frequencies in $Ru(py)_6^{2+}$ and $Ru(py)_6^{3+}$, an assumption consistent with the results for analogous tris(bpy) complexes,[26] the reduced force constant for the Ru−N(py) stretching vibration is 3.0×10^5 dyn cm^{-1}. Assuming further that these force constants are applicable to the $(NH_3)_5Ru^{II}L^{n+}/(NH_3)_5Ru^{III}L^{(n+1)+}$ couples yields eq 1b, where the bond distance differences are in angstroms and the reorganization energy is in kilocalories per mole. Equation 1b yields ΔG^*_{in} = 0.52, 1.12, 1.42, and 2.40 kcal mol^{-1} (λ_{in} = 2.1, 4.5, 5.7, and 9.6 kcal mol^{-1}) for the pyridine, benzonitrile, pyrazine, and *N*-methylpyrazinium self-exchanges, respectively. The inner-shell reorganization energies are not large, and the activation barriers for the electron exchange reactions of these couples will be dominated by the solvent reorganization, at least in polar solvents.[27] Nevertheless, the inner-shell barriers for the pyrazine and *N*-methylpyrazinium couples are not insignificant, amounting to 1−2 orders of magnitude in their self-exchange rates.

Table 4. Inner-Shell Reorganization Energies (λ_{in}) for the $(NH_3)_5Ru^{II}L^{n+}/(NH_3)_5Ru^{III}L^{(n+1)+}$ Self-Exchange Reactions

	λ_{in}, kcal mol^{-1}			
L	eq 1b	MM2	ZINDO[a]	ZINDO[b]
pyridine	2.1	3.9	4.2	4.2
benzonitrile	4.5	7.6	7.8	7.6
pyrazine	5.7	9.6	11.3	10.4
N-methylpyrazinium	9.6	15	14.6	11.8

[a] Reorganization energy from eq 1a using harmonic force constants calculated from the energy required to stretch the five Ru−NH_3 bonds in phase and to independently stretch the Ru−N(L) bond in the energy-minimized structure. [b] Reorganization energy equal to twice the difference in the energies of the distorted and undistorted (energy-minimized) structures.

$$\Delta G^*_{in} = 35.7[3.0(\Delta d^0(Ru-N(L)))^2 + 8.8(\Delta d^0(Ru-N_{eq}))^2 + 2.2(\Delta d^0(Ru-N_{ax}))^2] \qquad (1b)$$

The λ_{in} values calculated above may be compared with the inner-shell reorganization energies obtained by the molecular mechanics calculations. The inner-shell reorganization energies calculated by the CAChe MM program (Table 4) are some 60−100% larger than the values calculated from eq 1b. Reorganization energies were also calculated using ZINDO-95. Energy-minimized structures of the $(NH_3)_5Ru^{II}L^{n+}$ complexes were first generated using the ZINDO geometry optimization routine.[28] The energies of the complexes were then calculated as a function of their Ru−N distances using the same interaction factors as in the geometry optimization. The five Ru−NH_3 bonds were stretched in-phase, and the resulting energy curves were fitted

(20) Piarulli, U.; Floriani, C.; Chiesi-Villa, A.; Rizzoli, C. *J. Chem. Soc., Chem. Commun.* **1994**, 895−896.
(21) Duff, C. M.; Heath, G. A.; Willis, A. C. *Acta Crystallogr.* **1990**, *C46*, 2320−2324.
(22) Sutin, N. *Prog. Inorg. Chem.* **1983**, *30*, 441−498.
(23) Griffith, W. P. *J. Chem. Soc. A* **1966**, 899−901.
(24) Deak, A.; Templeton, J. L. *Inorg. Chem.* **1980**, *19*, 1075−1077.
(25) Templeton, J. L. *J. Am. Chem. Soc.* **1979**, *101*, 4906−4917.
(26) Saito, Y.; Takemoto, J.; Hutchinson, B.; Nakamoto, K. *Inorg. Chem.* **1972**, *11*, 2003−2011.
(27) Brown, G. M.; Sutin, N. *J. Am. Chem. Soc.* **1979**, *101*, 883−892.
(28) Reorganization energies are defined as the energy difference between the reactants in their equilibrium nuclear configuration and when they are at the equilibrium nuclear configuration of the products. Neither the MM2 force field nor ZINDO predicts an energy-minimized structure of $(NH_3)_5RuL^{2+}$ that has the observed bond lengths. To calculate the reorganization energy, the geometry of the complex was first optimized using MM or ZINDO, and the energy difference between this minimized structure and the structure distorted by the observed Ru−N bond distance differences between the Ru(III) and Ru(II) complexes was then calculated. No attempt was made to optimize the parameters in either MM2 or ZINDO to obtain the observed structures.

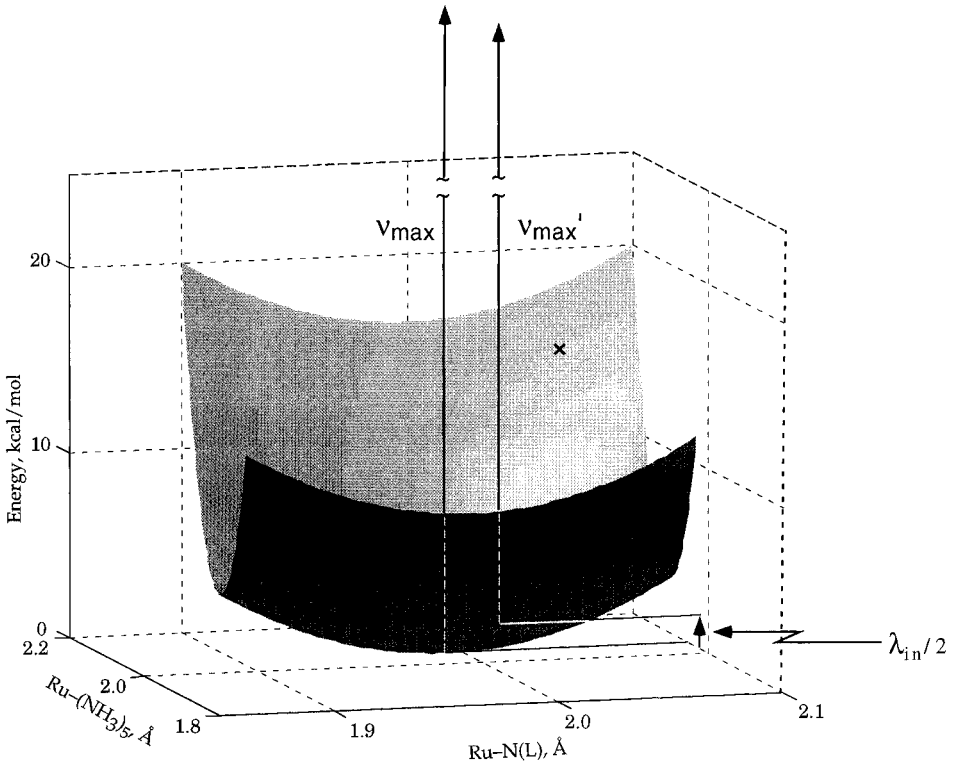

Figure 3. Ground-state energy surface of $(NH_3)_5Ru(py)^{2+}$ in vacuum. The minimum in the ground-state surface is located at the coordinates calculated with the ZINDO geometry optimization routine. The Ru−N bond lengths of the energy-minimized structure are 1.992, 2.052, and 2.062 Å for the pyridine, the equatorial NH_3's, and the axial NH_3, respectively. The latter distances were averaged to yield a mean Ru−NH_3 bond length of 2.054 Å. The stretching force constants for the Ru−py and Ru−NH_3 bonds were calculated to be 5.9×10^5 and 4.7×10^5 dyn cm^{-1}, respectively. These force constants, with the five Ru−NH_3 bonds stretching in phase, were used to construct the ground-state surface. The coordinates and energy of the structure determined in the X-ray measurements are indicated by ×. The MLCT transitions from the energy minimum and from the distorted $(NH_3)_5Ru(py)^{2+}$ configuration are also shown. The latter configuration was obtained by adding the difference between the metal−ligand distances (obtained from the X-ray crystal structure determination) of the Ru(III) and Ru(II) complexes to those of the energy-minimized structure.

to quadratics. This procedure yielded Ru^{II}−N stretching force constants of $\sim 5 \times 10^5$ dyn cm^{-1}, significantly higher than those estimated above from infrared and Raman data but close to the value used in the CAChe molecular mechanics program (4.4×10^5 dyn cm^{-1}). The calculated energy surface for $(NH_3)_5Ru(py)^{2+}$ is shown in Figure 3. Note that the minimum in the ZINDO-generated surface does not coincide with the Ru^{II}−N distances determined in the X-ray measurements, indicated by × in the figure. λ_{in} values were calculated from eq 1a with the assumption that the ZINDO stretching force constants are independent of ruthenium oxidation state. Not surprisingly, in view of the higher force constants used, the derived λ_{in} values (Table 4) are larger than those calculated from eq 1b. Also included in Table 4 are λ_{in} values calculated from the difference in the energies of the energy-minimized Ru(II) complex and the complex distorted by Δd^0 as a model for the coordinates of the Ru(III) complex. This approach yields somewhat lower reorganization energies than the harmonic ZINDO approximation for the complexes with the larger structural changes, perhaps reflecting limitations in the harmonic approximation and/or the approximation of treating the Ru−NH_3 and Ru−N(L) bond stretches independently. However, the differences are not large, and overall the inner-shell reorganization energies calculated by the semiempirical and molecular mechanics methods are in good agreement. Moreover, in the worst case, the difference in the reorganization energies calculated from eq 1b and by the semiempirical methods amounts to only about an order of magnitude in self-exchange rate.

Finally, comparisons can be made with the inner-shell reorganization energies derived from the measured self-exchange rates and also from the energies of the metal-to-metal charge transfer (MMCT) transitions in appropriate binuclear systems. Self-exchange rate constants and the energies of MMCT transitions yield total reorganization energies $\lambda = \lambda_{in} + \lambda_{out}$. The inner-shell reorganization energy of interest is then obtained from $\lambda - \lambda_{out}$, i.e., as a small difference between two relatively large numbers. In addition, a model for λ_{out} is required. For the present systems, self-exchange data are available only for the $(NH_3)_5Ru(py)^{2+/3+}$ couple. From the measured self-exchange rate, 1.1×10^5 M^{-1} s^{-1} at 25 °C,[27] and the semiclassical electron-transfer model for spherical reactants (two-sphere model, average reactant radius 4.03 Å[29] and average electronic transmission coefficient 0.33[30]), λ and λ_{out} are calculated to be 30 and 23 kcal mol^{-1}, respectively. Accordingly, $\lambda_{in} \approx 7$ kcal mol^{-1}. A somewhat different model that assumes the electron exchange proceeds by py−py contact (metal−metal separation distance 13.6 Å and electronic transmission coefficient 1.0) yields $\lambda_{in} \approx 6$ kcal mol^{-1}. Alternatively, λ_{in} can be estimated from the solvent dependence of the MMCT transition in $[(NH_3)_5Ru^{II}(4,4'\text{-bpy})Ru^{III}(NH_3)_5]^{5+}$. The intercept of the plot of the energy of the MMCT transition vs $(1/D_{op} - 1/D_s)$ yields $\lambda_{in} \approx 6$ kcal mol^{-1} after correction for spin−orbit coupling.[29] The various "experimental" estimates of λ_{in} are in surprisingly good agreement. Moreover, they are in satisfactory agreement with the values calculated by the MM and ZINDO methods (Table 4).

Dependence of the Spectroscopic Parameters on Metal−Ligand Distance. The $(NH_3)_5Ru^{II}L^{n+}$ complexes considered above exhibit intense metal-to-ligand charge transfer (MLCT)

(29) Brunschwig, B. S.; Ehrenson, S.; Sutin, N. *J. Phys. Chem.* **1986**, *90*, 3657−3668.

(30) The electronic transmission coefficient of 0.33 is a weighted average of $\kappa_{el} = 0.2$ for Ru(NH_3)−(NH_3)Ru and $\kappa_{el} = 1.0$ for Ru(py)−(py)-Ru contact.[22]

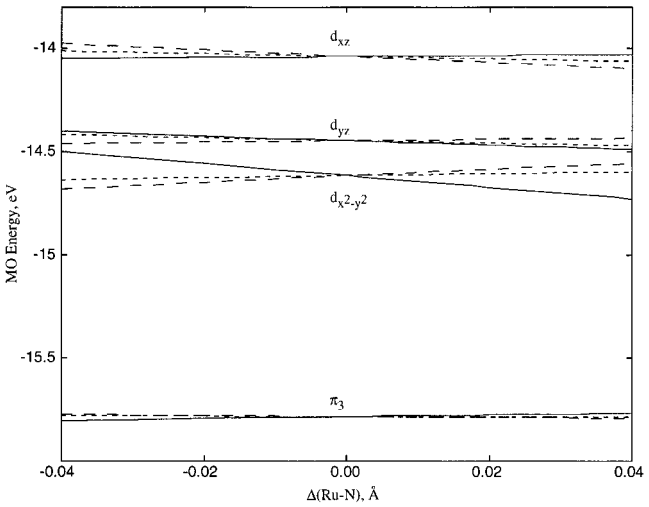

Figure 4. Effect of changing the Ru−N bond lengths from their energy-minimized values on the molecular orbital energies of ground-state $(NH_3)_5Ru(py)^{2+}$ in vacuum. The Ru−N(py), Ru−$(NH_3)_{eq}$, and Ru−$(NH_3)_{ax}$ distances are indicated by long dashes, solid lines, and short dashes, respectively.

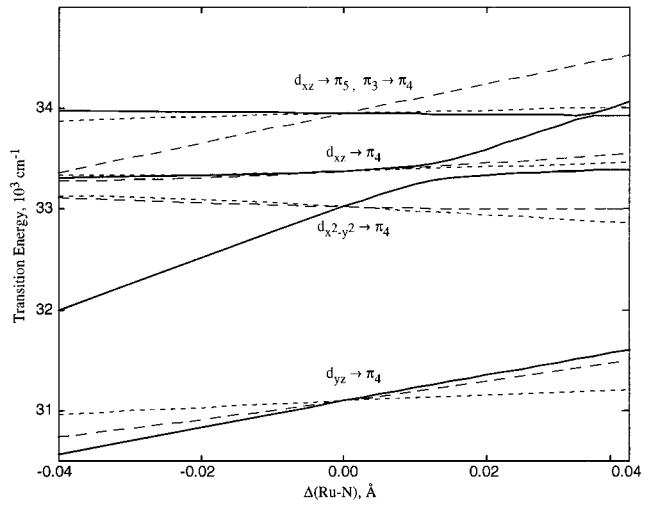

Figure 5. Effect of changing the Ru−N bond lengths from their energy-minimized values on the calculated MLCT transition energies for $(NH_3)_5Ru(py)^{2+}$ in vacuum. The Ru−N(py), Ru−$(NH_3)_{eq}$, and Ru−$(NH_3)_{ax}$ distances are indicated by long dashes, solid lines, and short dashes, respectively.

transitions in the visible region of the spectrum. The dependence of the energies and oscillator strengths of the MLCT transitions in the pyridine complex on the Ru−N distances was evaluated using the ZINDO CI option. The coordinate system introduced earlier[31] was used: the C_2 axis defines the z axis, and the pyridine plane defines the yz plane; d_{xz} is the ruthenium t_{2g} orbital that interacts strongly with the pyridine π system, and d_{yz} and $d_{x^2-y^2}$, previously denoted by $d_{\pi'}$ and d_δ, respectively, are the other t_{2g} orbitals. As shown recently,[31] the d_{xz} orbital is the HOMO, and the $d_{xz} \rightarrow L_{\pi 4}$ charge transfer is the MLCT transition with the greatest oscillator strength at the Ru−N distances determined in the X-ray measurements.

The effects on the molecular orbital (MO) and MLCT energies of changing the Ru−N distances from their energy-minimized values by ±0.04 Å are shown in Figures 4 and 5. The solid lines show the effect of changing the equatorial Ru−NH_3 distances from 2.052 Å. The d_{xz} orbital remains the HOMO, its energy remains essentially unchanged (Figure 4),

(31) Shin, Y.-g. K.; Brunschwig, B. S.; Creutz, C.; Newton, M. D.; Sutin, N. *J. Phys. Chem.* **1996**, *100*, 1104−1110.

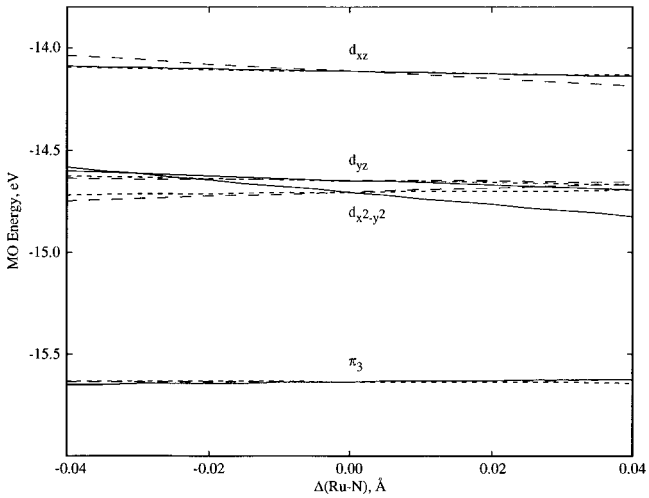

Figure 6. Effect of changing the Ru−N bond lengths from their measured values on the molecular orbital energies of ground-state $(NH_3)_5Ru(py)^{2+}$ in vacuum. The Ru−N(py), Ru−$(NH_3)_{eq}$, and Ru−$NH_3)_{ax}$ distances are indicated by long dashes, solid lines, and short dashes, respectively.

and the energy of the $d_{xz} \rightarrow L_{\pi 4}$ transition is also unchanged (Figure 5). The energies of the d_{yz} and particularly the $d_{x^2-y^2}$ orbitals and the energies of the $d_{yz} \rightarrow L_{\pi 4}$ and $d_{x^2-y^2} \rightarrow L_{\pi 4}$ transitions are more sensitive to the equatorial bond lengths. As is evident from Figure 5, mixing of the excited states formed in the "pure" $d_{xz} \rightarrow L_{\pi 4}$ and $d_{x^2-y^2} \rightarrow L_{\pi 4}$ transitions occurs when the equatorial Ru−NH_3 distances are increased to about 2.072 Å (Δ(Ru−N) = +0.020Å). The $d_{x^2-y^2} \rightarrow L_{\pi 4}$ transition becomes the dominant component of the higher energy transition at longer equatorial Ru−NH_3 distances. However, only the $d_{xz} \rightarrow L_{\pi 4}$ transition has significant oscillator strength, and the $d_{x^2-y^2} \rightarrow L_{\pi 4}$ transition has intensity only when the two excited states mix.

The effect of changing the Ru−N(py) distance from its energy-minimized value of 1.992 Å on the MO and MLCT energies is shown by the long dashes in Figures 4 and 5. The d_{xz} orbital remains the HOMO throughout the Ru−N(py) distance change: its energy decreases, while that of the $d_{x^2-y^2}$ orbital increases, with increasing Ru−N(py) separation. The energy of the mixed $d_{xz} \rightarrow L_{\pi 5}$, $L_{\pi 3} \rightarrow L_{\pi 4}$ transition (Figure 5) is quite sensitive to the Ru−N(py) distance. Except for the smaller dependence of the energy of the $d_{xz} \rightarrow L_{\pi 5}$, $L_{\pi 3} \rightarrow L_{\pi 4}$ transition on the axial Ru−NH_3 distance, similar effects on the MO and MLCT energies are observed upon changing the axial Ru−NH_3 distance (short dashes) from its energy-minimized value of 2.062 Å.

For comparison, the effects on the MO and MLCT energies of changing the Ru−N bond lengths from their *measured values* by ±0.04 Å are shown in Figures 6 and 7. The MO scheme is similar to that for the energy-minimized structure. The d_{xz} orbital remains the HOMO, but there is somewhat less separation between the $d_{x^2-y^2}$ and d_{yz} orbitals in the X-ray structure, consistent with its longer Ru−N distances. All of the MLCT transitions have moved to *higher* energies at the measured Ru−N distances compared with the energy-minimized structure. As in the energy-minimized structure, the only MLCT transition with significant oscillator strength is the $d_{xz} \rightarrow L_{\pi 4}$ transition. The $d_{x^2-y^2} \rightarrow L_{\pi 4}$ MLCT transition mixes with the d−d transitions at longer equatorial Ru−NH_3 distances. It should be recalled that the Ru^{II}−NH_3 bonds (solid lines and short dashes) are longer and the Ru^{II}−N(py) bonds (long dashes) are shorter than the corresponding bonds in the Ru(III) complexes. There is mixing of the $d_{xz} \rightarrow L_{\pi 5}$, $L_{\pi 3} \rightarrow L_{\pi 4}$ with the $d_{xz} \rightarrow L_{\pi 4}$

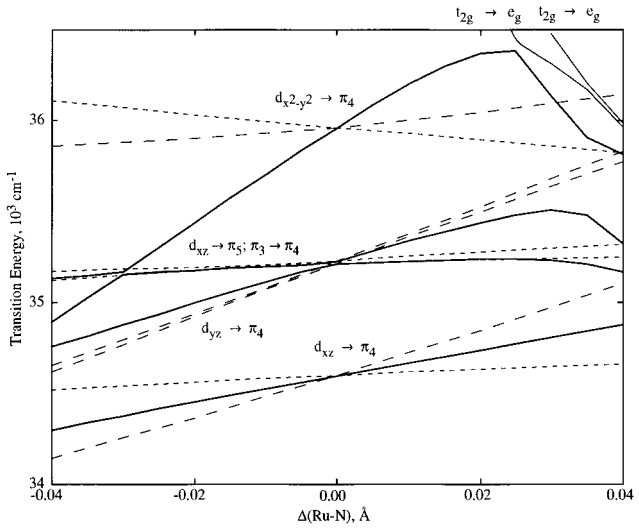

Figure 7. Effect of changing the Ru−N bond lengths from their measured values on the calculated MLCT transition energies for $(NH_3)_5Ru(py)^{2+}$ in vacuum. The Ru−N(py), Ru−$(NH_3)_{eq}$, and Ru−$(NH_3)_{ax}$ distances are indicated by long dashes, solid lines, and short dashes, respectively.

transitions at the measured Ru^{II}−N distances and with the $d_{x^2-y^2} \rightarrow L_{\pi 4}$ transitions at shorter Ru−$(NH_3)_{eq}$ distances, but none of these transitions has significant intensity. To summarize, the d_{xz} orbital remains the HOMO, and, except when mixed with transitions that borrow intensity from it, the $d_{xz} \rightarrow L_{\pi 4}$ charge transfer remains the most intense MLCT transition over the entire range of Ru−N distances considered.

Metal−Ligand Coupling Elements. The metal−ligand coupling element, H_{ML}, is another important quantity that characterizes the strength of the metal−ligand interaction. The coupling elements can be related to the energies and intensities of the MLCT transitions and the charge transfer distance using the Mulliken−Hush formalism. H_{ML} values determined in this manner are typically 7000−10 500 cm^{-1} for $(NH_3)_5Ru^{II}L$ and 2000−3500 cm^{-1} for $(NH_3)_5Ru^{III}L$ complexes (L = an aromatic N-heterocycle or a cyanobenzene derivative).[32]

Coupling elements were calculated for the complexes without solvating water molecules and with 15 water molecules located along the N−H bond axes with the O atom of each water molecule 2.8 Å from the N.[31] The coupling elements were obtained from eq 2, where ν_{max} is the MLCT absorption band

$$H_{ML} = \left| \frac{\nu_{max}\mu_{ge}}{(\mu_b - \mu_a)} \right| \quad (2a)$$

$$(\mu_b - \mu_a)^2 = (\mu_e - \mu_g)^2 + 4(\mu_{ge})^2 \quad (2b)$$

maximum, μ_{ge} is the transition dipole moment, $\mu_b - \mu_a$ is the difference between the dipole moments of the localized (diabatic) states, and $\mu_e - \mu_g$ is the corresponding difference for the delocalized (adiabatic) states.[32,33] The experimental H_{ML} values were obtained from the measured values of ν_{max} and μ_{ge} and values of $\mu_e - \mu_g$ determined in Stark measurements.[32] The experimental and calculated MLCT transition energies, oscillator strengths, and coupling elements are presented in Table 5. As found for other complexes of the family,[31] the MLCT transition energies are appreciably overestimated. While hydration of the complexes decreases the calculated transition energies, they are still substantially larger than the experimental values. With the exception of that of the benzonitrile complex, the oscillator strengths are also overestimated. The experimental H_{ML} values for the complexes are all similar and at the high end of the H_{ML} range noted above. H_{ML} for the *N*-methylpyrazinium complex is $\sim\nu_{max}/2$, consistent with a delocalized ground state. The calculated H_{ML} values tend to be somewhat larger than the experimental values, with the disagreement arising primarily from the differences between the experimental and calculated transition energies noted above. Not surprisingly, the agreement tends to be somewhat better for the hydrated complexes. Somewhat better agreement with the experimental MLCT transition energies is found for the energy-minimized geometries, with the agreement being best for the benzonitrile complex.

Table 5. Experimental and Calculated Spectroscopic Parameters and Metal−Ligand Coupling Elements [a]

	exptl, 77 K	in vacuum: Ru(II) X-ray	in vacuum: Ru(II) E_{min} [b]	in vacuum: Ru(II)′ reorg [c]	with 15H_2O, Ru(II) X-ray
		$(NH_3)_5Ru^{II}(py)^{2+}$			
ν_{max}/kK	23.1	34.6	33.4	33.2	29.6
λ_{max}/nm	433	289	300	301	338
f_{os}	0.15	0.38	0.47	0.47	0.45
$\lvert\mu_{ge}\rvert$/D	3.8	4.8	5.5	5.5	5.7
$\lvert\mu_e - \mu_g\rvert$/D	3.4	10.2	9.1	9.5	11.0
$\lvert\mu_b - \mu_a\rvert$/D	8.3	14.0	14.2	14.5	15.8
H_{ML}/kK	10.5	11.9	12.9	12.6	10.7
		$(NH_3)_5Ru^{II}(NCC_6H_5)^{2+}$			
ν_{max}/kK	25.4	31.8	28.4	29.4	30.2
λ_{max}/nm	394	315	353	340	331
f_{os}	0.26	0.19	0.16	0.19	0.15
$\lvert\mu_{ge}\rvert$/D	4.6	3.6	3.5	3.7	3.2
$\lvert\mu_e - \mu_g\rvert$/D	8.7	5.2	5.1	5.4	8.0
$\lvert\mu_b - \mu_a\rvert$/D	12.7	8.9	8.7	9.2	10.2
H_{ML}/kK	9.2	12.9	11.5	11.9	9.4
		$(NH_3)_5Ru^{II}(pz)^{2+}$ [d]			
ν_{max}/kK	20.1	32.8	32.6	32.1	29.7
λ_{max}/nm	498	305	306	312	337
f_{os}	0.20	0.49	0.54	0.46	0.52
$\lvert\mu_{ge}\rvert$/D	4.6	5.7	5.9	5.5	6.1
$\lvert\mu_e - \mu_g\rvert$/D	3.5	9.5	8.8	10.3	8.8
$\lvert\mu_b - \mu_a\rvert$/D	9.8	14.8	14.7	15.1	15.0
H_{ML}/kK	9.4	12.5	13.1	11.7	12.0
		$(NH_3)_5Ru^{II}(pzCH_3^+)^{3+}$ [d]			
ν_{max}/kK	18.7	28.3	27.3	24.9	28.0
λ_{max}/nm	535	354	366	401	358
f_{os}	0.27	0.94	0.86	0.66	1.13
$\lvert\mu_{ge}\rvert$/D	5.5	8.4	8.2	7.5	9.5
$\lvert\mu_e - \mu_g\rvert$/D	2.0	5.6	7.3	10.9	3.3
$\lvert\mu_b - \mu_a\rvert$/D	11.2	17.7	18.0	18.6	19.3
H_{ML}/kK	9.2	13.4	12.4	10.1	13.8

[a] ν_{max} and λ_{max} are the energy and wavelength of the MLCT absorption maximum, respectively, and f_{os} is the oscillator strength of the MLCT transition. [b] Calculated for the $(NH_3)_5Ru^{II}L^{n+}$ geometry obtained by ZINDO energy minimization. [c] Calculated for the vibrationally excited Ru(II) configuration obtained by distorting the geometry-optimized $(NH_3)_5Ru^{II}L^{n+}$ structure by the difference between the equilibrium geometries of the Ru(II) and Ru(III) complexes. [d] High-energy MLCT transition.

The metal−ligand coupling elements enter into superexchange expressions for the metal-to-metal coupling, H_{MM}, in weakly coupled ligand-bridged binuclear systems (eq 3). The dependence of the coupling elements on the nuclear configurations of the complexes is, therefore, of considerable interest.[34] Since smaller bond distance changes are involved in distorting the complexes to their transition-state configurations, optical metal-

$$H_{MM} = \frac{H_{ML}H_{M'L}}{2\Delta E_{ML}} \quad (3)$$

(32) Shin, Y.-g. K.; Brunschwig, B. S.; Creutz, C.; Sutin, N. *J. Phys. Chem.* **1996**, *100*, 8157−8169.
(33) Cave, R. J.; Newton, M. D. *Chem. Phys. Lett.* **1996**, *249*, 15−19.

to-metal charge transfer (MMCT) will be considered. In optical MMCT, H_{ML} is the metal−ligand coupling element for $(NH_3)_5Ru^{II}L^{n+}$ at the Ru^{II}−N equilibrium configuration, $H_{M'L}$ is the corresponding quantity for a $(NH_3)_5Ru^{II}L^{n+}$ at the Ru^{III}−N geometry, and ΔE_{ML} is the effective metal−ligand energy gap.[35]

The nuclear coordinates of the Ru(II) complexes distorted to the corresponding Ru(III) configurations were obtained by correcting the energy-minimized Ru(II) configurations by Δd^0. The spectroscopic parameters calculated at the Ru(III) configurations are included in Table 5. The calculated MLCT transition energies for the unhydrated pyridine, pyrazine, and *N*-methylpyrazinium complexes follow the expected trend: they are lower for Ru(II) at the Ru(III) geometry than at its energy-minimized geometry (Figure 3), and the transition energy differences for the series follow the λ_{in} order in Table 4. Except for the benzonitrile complex, the $H_{M'L}$ values calculated at the Ru(III) geometry are somewhat smaller than the H_{ML} values calculated at the energy-minimized geometry, with the H_{ML} decreases paralleling the degree of distortion. The largest decrease is only ∼20%, consistent with the relatively small structural changes involved. The anomalous result for the benzonitrile complex derives from the *higher* transition energy calculated for the distorted structure. Consequently the transition energy, ν_{max}', for the distorted benzonitrile complex was estimated from $\nu_{max}', = \nu_{max} - \lambda_{in}$, where ν_{max} is the transition energy for the undistorted complex (Figure 3), and substituted into eq 2 to estimate $H_{M'L}$ for the distorted complex. This procedure yields a ∼2% decrease in H_{ML} upon distortion of the Ru(II) benzonitrile complex to the Ru(III) configuration, in line with the coupling element decreases for the other complexes. As noted above, an even smaller change of the metal−ligand coupling element is expected to be associated with the reorganization involved in thermal MMCT. The results for the $(NH_3)_5Ru^{II}L^{n+}$ series thus justify neglect of the nuclear configuration dependence of H_{ML} in calculating Ru(II)−Ru(III) coupling elements in weakly coupled $[(NH_3)_5Ru^{II}LRu^{III}(NH_3)_5]^{n+}$ complexes.

Conclusions

With the determination of the structures of the pyridine and benzonitrile complexes reported here, a comprehensive set of structural parameters for modeling and interpreting electron transfer barriers and for investigating the dependence of metal−ligand coupling on d_{Ru-N} are available for L = pyridine, benzonitrile, pyrazine, and *N*-methylpyrazinium. The inner-shell reorganization energies (λ_{in} = 2.1, 4.5, 5.7, and 9.6 kcal mol^{-1}, respectively) are not large, and as a consequence the activation barrier for the electron exchange reactions of the $(NH_3)_5RuL^{2+}/(NH_3)_5RuL^{3+}$ couples will be dominated by the solvent reorganization, at least in polar solvents. Nevertheless, the inner-shell barriers for the pyrazine and *N*-methylpyrazinium couples are not insignificant, amounting to an order of magnitude in their self-exchange rates. INDO calculations for $(NH_3)_5Ru(py)^{2+}$ show that the d_{xz} orbital remains the HOMO and, except when mixed with transitions that borrow intensity from it, the $d_{xz} \rightarrow L_{\pi 4}$ charge transfer remains the most intense MLCT transition for changes of ±0.04 Å in both the X-ray-determined and the energy-minimized Ru−N distances. Finally, the INDO calculations for the $(NH_3)_5Ru^{II}L^{n+}$ series justify neglect of the dependence of H_{ML} on nuclear configuration in calculating the Ru(II)−Ru(III) interaction in weakly coupled $[(NH_3)_5Ru^{II}LRu^{III}(NH_3)_5]^{n+}$ complexes.

Acknowledgment. We thank Dr. M. D. Newton for valuable comments. This research was carried out at Brookhaven National Laboratory under Contract DE-AC02-76CH00016 with the U.S. Department of Energy and supported by its Division of Chemical Sciences, Office of Basic Energy Sciences.

Supporting Information Available: Tables S1−S19, giving additional experimental details, positional pasrameters, anisotropic thermal parameters, parameters for hydrogen atoms, complete listing of bond distances and angles, and proposed hydrogen bonds for **1**−**4** (31 pages). Ordering information is given on any current masthead page.

IC9700967

(34) Creutz, C.; Newton, M. D.; Sutin, N. *J. Photochem. Photobiol. A: Chem.* **1994**, *82*, 47−59.

(35) Strictly speaking, in applying eq 3 to optical MMCT in a symmetrical ligand-bridged binuclear system, the metal−ligand coupling element H_{ML} refers to the MLCT transition in the initial equilibrium state of the binuclear complex, $Ru^{II}_{II,equil}LRu^{III}_{III,equil}$, in the absence of metal−metal coupling. Similarly, $H_{M'L}$ refers to the MLCT transition in $Ru^{III}_{II,equil}LRu^{II}_{III,equil}$, formed in the (vertical) MMCT transition from the initial state, or, equivalently, in $Ru^{II}_{III,equil}LRu^{III}_{II,equil}$, formed by vibrational excitation of the initial state. The same doublet MLCT state, $Ru^{III}_{II,equil}L^{-}Ru^{III}_{III,equil}$, is formed in all three transitions. (More correctly, two excited doublet states, differing in the spin pairing of the three singly occupied orbitals, need to be considered.[34]) In any event, the Ru(III) may be regarded as part of ligand L, and its presence is not expected to significantly affect the conclusion regarding the nuclear configuration dependence of H_{ML}.